

# Detection of Synthetic Singularities in Natural Textures and Mammographies using Nearly Spherical Wavelets and filters

C. Gouttière, G. Lemaure & J. De Coninck

Université de Mons-Hainaut, C. R. M. M., Parc Initialis, Avenue Copernic 1,  
Bât. Materia Nova, 7000 Mons, Belgium

---

*The efficiency of defect detection for filters and wavelets is a fundamental problem in image processing. It has recently been shown that natural symmetries such as rotational invariance is of primary importance to solve this problem [1, 2]. We herewith investigate the detection of tunable singularities in natural textures from the Brodatz database and in parts of mammographies. We compare several filters and show that the efficiency of pointwise defect detection is intimately related to their rotational invariance property.*

**Keywords:** Image processing, Defect detection, Brodatz textures

---

## 1. INTRODUCTION

Image analysis is a very active field of research in computer science. Particularly, defect detection is the subject of numerous studies such as in the case of medical images for instance. It is well known that wavelet analysis is a very useful tool for extracting the singular part of a signal [3, 4]. There are however numerous types of images and equivalently numerous types of filters which can be used to analyse them. If we are interested by the optimization, either in time or in quality, of the defect detection, a natural question arises: how can we choose the appropriate filter? In practice, specific types of images (glasses, tiles, etc) can be well analysed by dedicated algorithms. Here we are more interested by a theoretical approach based on general properties of images or more precisely its symmetries. A local defect has to remain a defect even if we rotate the image for instance.

The regularity of wavelets has, from a long time, been one of the main criteria for building wavelet families, motivated for example by the above experiments. However, in [5], while studying the texture segmentation using wavelets, M. Unser found that the number of null moments (characterizing one aspect of the regularity) alone was not sufficient for choosing a wavelet. The most regular wavelet was not necessarily the best at distinguishing textures.

Another possibility to characterize the regularity of wavelets is through their Sobolev exponent [6]. In [7] and [8], it was shown that, among the Matzinger wavelets, which are good with respect to Sobolev regularity, the detection was improved with more regular wavelets. In [9], orthonormal wavelets of various lengths were optimized numerically for the Sobolev regularity.

Most of the wavelets families have mathematical properties which take their roots in some modeling of the signal. Either the signal is assumed locally polynomial (number of null moments) or lie in a smooth space (Sobolev space). In reality, very few signals follow some mathematical

model. This is why, in our opinion, a more intuitive understanding of the 2D signal may provide better results.

The choice of the best separable wavelet basis function for the extraction of image information has been addressed previously [10, 11] and particularly for singularity detection based on local sphericity [1, 2, 3, 4]. This new criterion proved useful for creating new wavelet filters: the nearly isotropic wavelets.

These new wavelets were compared to the Gabor filters and the Mexican hat filters in the aim to correlate their level of sphericity and their efficiency of detection for a rather large class of artificial defects represented by cones in synthetic images, like in Fig. 1. The conclusion of this study is that a more spherical filter detects the singularity defects with more efficiency, particularly in the case of the synthetic images with a high roughness background. An image with a larger roughness background seems more textured than another with a lower roughness background. The reason for using synthetic images for detection tests is the easy control of the roughness of the background of the images, which can be modified with a single parameter.

The practical interest of this study is the detection of small defects in medical images, like mammographies, for example. Indeed, a synthetic image with a high roughness background appears like a mammography, and the inserted conic defects appear like microcalcifications. From a medical point of view, it is very important to detect precociously these anomalies in order to treat the disease in its early phase. This is why we apply our detection methodology on a set of mammography parts.

An other application of this study can be the detection of small defects in textured images, as those captured from cameras along a production line in industry. This leads us to test our method of defect detection on natural textured images of reference. The Brodatz images<sup>1</sup> have been selected for our test.

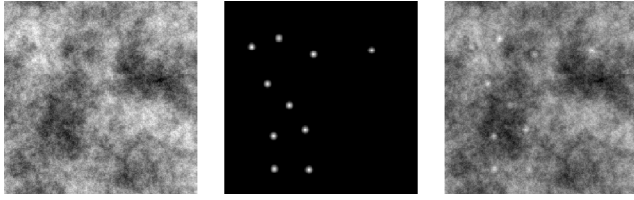


Figure 1: Example of synthetic image with controlled defects

The first experiment developed in this work concerns the detection of controlled singularities in the Brodatz textures and in parts of mammographies. To further investigate the problem of defect detection, it can be interesting to evaluate the importance of the singularity at the top of the cone. To this end, we change the defect model and use a cone with its top truncated. This is the object of the second experiment.

This paper is organized as follows. For completeness we will first sketch the wavelets and filters used in our experiments. Next we will briefly explain the two kinds of defects and the method used to determine the efficiency of filter detection. Finally, we will present the experiments and the obtained results.

## 2. INVESTIGATED WAVELETS AND FILTERS

The choice of a wavelet basis for defect detection is not an easy task. To work with 2D images, one usually takes wavelets designed for one dimensional processing and just uses the tensor product. This enables to take advantage of all the knowledge of the properties of wavelets accumulated in one dimension. Such properties are for example the number of vanishing moments, good frequency localization, short impulse response.

In the present paper, we compare the ability to detect narrow singularities in images on the basis of general symmetries of the defects such as their rotation invariance. This problem leads naturally to the study of Mexican hat and Gabor filters. We add to this piece of work a separable “nearly” spherical wavelet defined as follows.

A filter  $f(x, y)$  is isotropic if it verifies the following equation:

$$\forall x_1, x_2, y_1, y_2 \in \mathbb{R}: x_1^2 + y_1^2 = x_2^2 + y_2^2 \Rightarrow f(x_1, y_1) = f(x_2, y_2)$$

We deal here with discrete filters. We can therefore not verify this equation as it is because only few points of the plane will satisfy this relation. Since most, if not all, of the filters we will examine will not be truly isotropic, we must find another criteria to classify the filters.

The wavelets bases generally used in image processing are extension in two dimensions of wavelet defined in one dimension. The equation below depicts a filter  $F$  as an extension in 2 dimensions of the filter  $G$  in one dimension:

$$F(x, y) = G(x)G(y)$$

$F$  is then called a separable filter.

We can use this property to search for a better strategy to classify wavelet as more or less rotation invariant. We want  $F$  to be rotation invariant. That translates to:

$$\forall x_1, x_2, y_1, y_2 \in \mathbb{R}: x_1^2 + y_1^2 = x_2^2 + y_2^2 \Rightarrow G(x_1)G(y_1) = G(x_2)G(y_2)$$

It follows that the only possible  $G$  is of the form  $a^{b \cdot x^2}$ .

The Gaussian  $k \cdot e^{-x^2/\sigma}$  is a possible solution for  $G$  but this is not an orthonormal wavelet. Note that  $k$  is a constant used to normalize the function. To assess the sphericity of a function, we can thus convolve it with a Gaussian. The maximum absolute value of this convolution will be an indication of the best match between the function and the Gaussian. The  $\sigma$  of the Gaussian will be tuned to give the highest possible match. To give comparable results, we must normalize both the function to be evaluated and the Gaussian. The highest score we can then reach is 1. The measure of the sphericity of the filters will thus be based on the similarity these filters have with a Gaussian, the only separable filter which is isotropic.

To be complete, our method to construct new separable spherical wavelets is described in appendix A.

### 2.1 Gabor filters

The first examined family of filters is the Gabor filters. These filters are chosen in this work because they are often investigated in the texture analysis domain. Several researches have dealt with using the Gabor filters to improve the texture classification [10, 11], segmentation [12], features extraction [13], defect detection [14], etc. The main advantage of the Gabor filters is that they are easily tunable in scale and orientation.

The bank of filters can be obtained by dilation and rotation of a mother function which has the following form :

$$\psi(x, y) = \frac{1}{2\pi\sigma_x\sigma_y} \exp\left[-\frac{1}{2}\left(\frac{x^2}{\sigma_x^2} + \frac{y^2}{\sigma_y^2}\right)\right] \cos(2\pi Wx). \quad (1)$$

where  $W$  is the modulation frequency of the filter and  $\sigma_x, \sigma_y$  define the Gaussian envelope size.

### 2.2 Mexican Hat Filters

The second examined family of filters is the Mexican hat filters. Several applications are based on methods using Mexican hat filters like texture classification [15] or pattern recognition [16, 17]. The Mexican hat function is defined as follows:

$$\psi(x, y) = \left(1 - \frac{x^2 + y^2}{2\sigma^2}\right) e^{-\frac{x^2 + y^2}{2\sigma^2}}. \quad (2)$$

We must note that these filters have the disadvantage that they are not separable. The computational time required to construct these filters is thus more important than for separable filters. This factor is not taken into account for our experiments, because it is not the aim of the study.

### 2.3 Nearly Isotropic Wavelets

The nearly isotropic wavelets have been specially developed to detect singularities [3, 4]. The construction of these wavelets is based on the optimisation of the sphericity of

the wavelet or the scaling function. The parametrization of the wavelets is achieved using the algorithm developed by Sherlock and Monro [18]. This can generate any kind of orthonormal wavelets.  $(N/2-1)$  parameters are free if the support width of the wavelet is  $N$ . The wavelet filter related to an isotropic wavelet function is denoted by  $\psi$  and the filter related to an isotropic scaling function is denoted by  $\phi$ . These wavelets have a support width of 8 so as to obtain the best trade-off between the sphericity and the length of the filter. The details of their construction can be found in [4]. The scaling functions of these two wavelet filters are represented in Fig. 2.

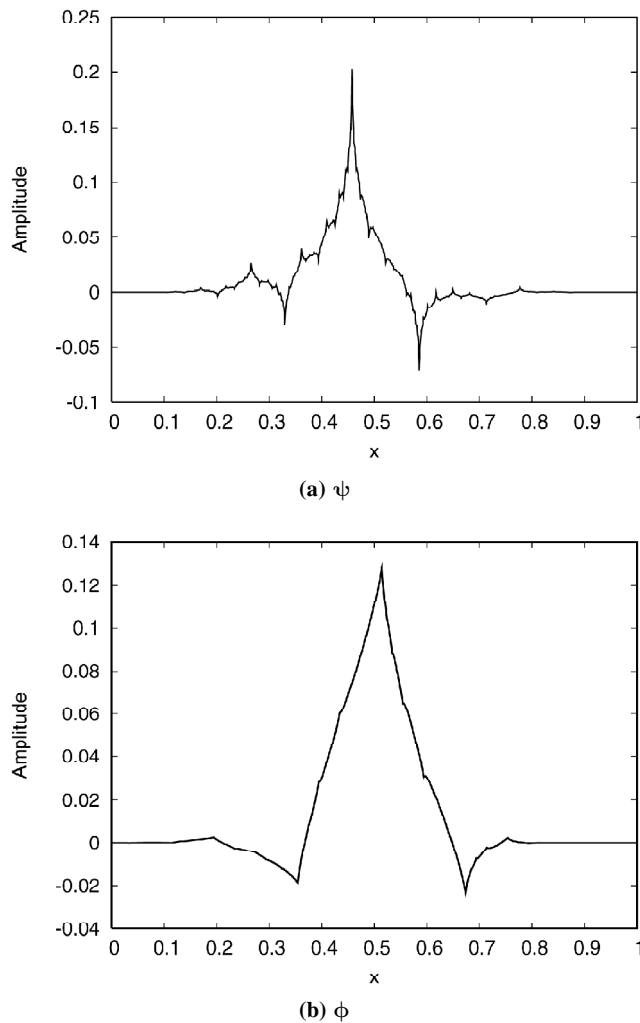


Figure 2: Scaling function of the wavelet filters

One of the possible applications of such a wavelet filter concerns medical image analysis, particularly the detection of clustered microcalcifications in mammograms [3, 8].

### 3. SINGULARITY AND TRUNCATED DEFECTS DETECTION

Our aim of using wavelet is to detect pointwise singularities. Since we do not assume some mathematical properties of the wavelet, we will choose the most simple defect: the signal is continuous while its first derivative is not.

In one dimension, we could choose the top of a triangle. Two possibilities can be used to generalize this to two dimensions: the tensor product of two 1D functions or the rotation of the triangle around an axis passing through the singularity. The second approach was considered, since the first one introduces two ridges along the axis, so that the pointwise singularity is at the crossing of two 1D singularities.

Rotating the triangle around its summit, we get a cone (we view the images as a profile, the intensity being mapped to the height of the landscape).

In this section we explain the singularity and truncated defect detection procedure. First we will describe the kind of defects we want to detect. Next we will show examples of images we want to process. Finally we will determine a measure of efficiency for the detection. We can note that the method of defect detection used in this work is the same as used in previous studies [1, 2]. We recapitulate this method in the following sections.

#### 3.1 Defect Creation

The first step is to detect singularity defects. To do this we create synthetic defects in the images. The form of the defects is a cone, which is formulated as follows:

$$D(x, y) = \max \left\{ 0, 1 - \left\| \begin{pmatrix} x \\ y \end{pmatrix} - \begin{pmatrix} c_x \\ c_y \end{pmatrix} \right\| R^{-1} \right\}, \quad (3)$$

where  $R$  is the radius of the base of the cone and  $(c_x, c_y)$  the position of its center.

The radius and the height of the defects can be changed. We can thus study the influence of the size of the defects on the efficiency of the detection by modifying the radius. The limit of the detection can then be determined by varying the height. As the second step, the cones are truncated at a percentage of their maximal height and the principle of the detection is similar to the detection of the cones. Examples of these two kinds of defects are shown in Fig. 3. Indeed, the first image (a) corresponds to a singularity defect with a radius of 100 pixels, the second one (b) to the first defect with the singularity truncated at 70% of the height, and the last one (c) to the first defect with the singularity truncated at 40% of the height. The corresponding 3-d views of these defects are shown respectively in (d), (e) and (f).

#### 3.2 Measure of Efficiency

Let us suppose that we have a clear image  $I$  which is a texture from the Brodatz database or a part of mammography. A sample texture images can be found in Fig. 4 from the Brodatz database and in Fig. 5 for mammography parts. Let us also suppose that we have an image containing singularity defects denoted  $D$ .

The tool we will use throughout this paper to evaluate the efficiency to detect singularities is the less intense defect, i.e. smallest intensity of the defect, we can segment from the background with a given probability of failure. To do

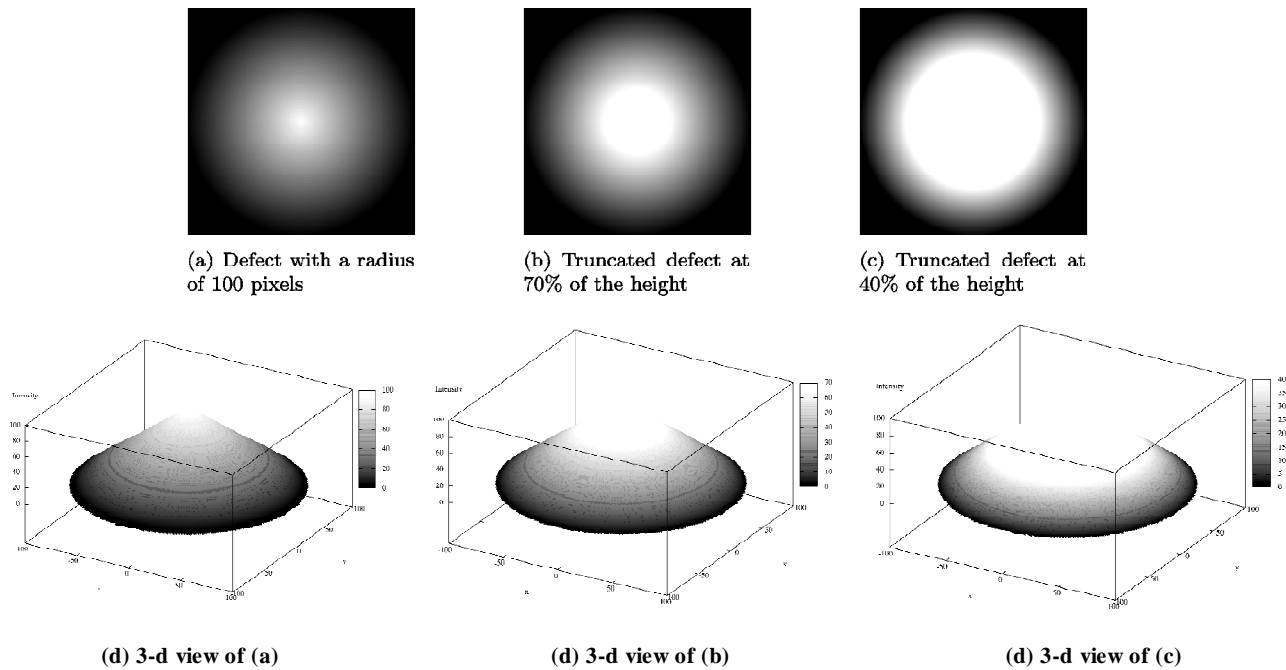


**Figure 3: Example of singularity and small sized defects, and their 3-d representation**

that, we first transform the original texture on several scales of the wavelet transform. We use a redundant transform to achieve better results. We can then fix a threshold given the acceptance rate of false positive. Let us note  $\tau$  this threshold.  $\tau$  depends on the texture, the wavelet base and the level of decomposition.

We then randomly add some defects. Of course, we record the position of these defects so as to be able to determine if the defect is detected or not. We say a defect is detected if the coefficient of the wavelet transform near the position of the defect is higher than  $\tau$ . We define “near” as being at most at one pixel from the position of the defect. This is to ensure we do not underestimate the wavelet for a small error in the localisation of the defect. We then adjust the heights of the defects so that the given error rate is achieved, in introducing a parameter  $\Omega$  which multiplies the image  $D$ . In summary, the procedure to compute  $\Omega$  for a given background is

- $F$  = background image,
- $D$  = set of 10 randomly positioned defects,
- Compute  $\Omega$  such that the wavelet can detect 9 defects on  $F + \Omega D$  with a false positive rate of  $\tau$ .

A value of  $\Omega$  close to 1 corresponds to a final image  $I + \Omega D$  where the defects can be easily distinguished. An example of  $I$ ,  $D$  and  $I + \Omega D$  can be found in Fig. 6 with the texture D1 from the Brodatz database, 10 conic defects with a radius equal to 5 pixels and  $\Omega$  equal to 0.3. An other example with a mammography part is shown in Fig. 7.

The problem is to detect significant singularities. The wavelet transform gives maximum response near the singularity at fine scales. Though, the noise is usually much more present at the finest scales. Therefore, our algorithm proceeds as follows. First, the wavelet transform is

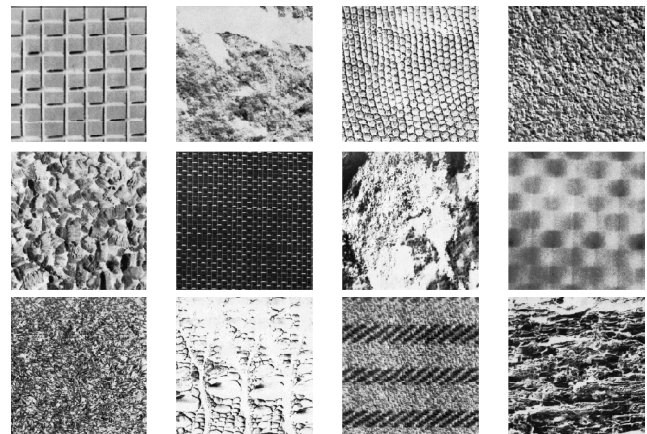


**Figure 4: Sample textured images from the Brodatz database**

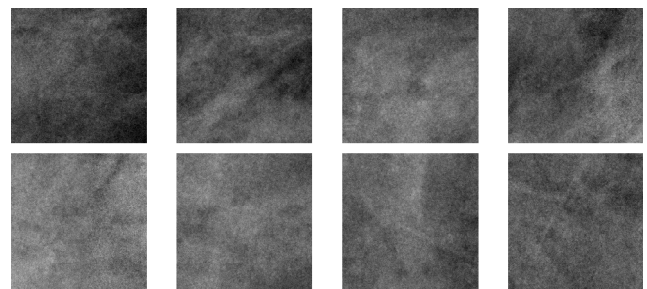
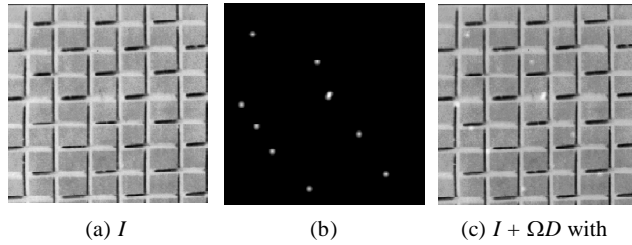


**Figure 5: Sample parts of mammographies**

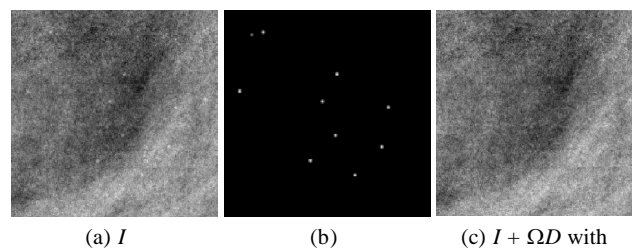
performed through several scales (here 4). To avoid the translation variance of the wavelet transform, the overcomplete transformation is used, i.e. no decimation is performed between scales. Then, given a threshold, the image is segmented. So, on the segmented image, we count a good detection if, near the location of the inserted defect (known, since artificially added), the wavelet transform is above the threshold.

Of course, the rate of good detection will greatly depend on the chosen threshold. Working with controlled images, it is possible to transform the defect free image and set the threshold such that only a few parasites appear, i.e. only a few points are falsely detected as singularities.



Defects Dwithradiuso of 5 pixels = 0.3

**Figure 6: Example of Brodatz image to be itered**



Defects Dwithradiuso of 3 pixels = 0.2

**Figure 7: Example of mammography part to be itered**

The best scale is then chosen, that is the scale at which the number of good detections is the highest while maintaining the number of parasites below some chosen value.

To summarize, we first process a clean image  $I$  so as to compute the threshold. The accepted parasite fraction is 0.1%. Then, 10 artificial defects are produced, giving the image  $D$ . The transform of  $I + \Omega D$  gives  $T$ . We then compute the rate of good detection and adjust  $\Omega$  such that 9 out of 10 defects are correctly segmented. This gives us the measure of the smallest defect the wavelet can detect. The transform can be done at different scales so we take the best scale for the evaluated wavelet.

This method to determine the value of efficiency of the detection is the same for both the cones and the truncated cones.

## 4. EXPERIMENTS AND RESULTS

In this section we first review the different filters and their associated parameters. We also determine the size of the defects to be detected and the method of truncation. We finally compare all the examined filters.

### 4.1 Values of the Parameters Defined in the Experiments

The first set of test images is composed of 110 textured images of size  $256 \times 256$  pixels collected from the Brodatz database. 30 parts of mammographies constitute the second set of test images. The inserted singularities in these images have a radius varying from 1 to 10 pixels. For the truncated defects, the truncation is performed between 10 and 100%

of the maximal height of the cone. The truncation at 100% corresponds to the whole cone. We insert 10 defects for each experiment. The random position of these 10 defects is the same for all of the 110 Brodatz images, and the other random position of the defects is also the same for all images of the second set. The use of 10 defects can be justified since tests were performed for 5 other positions and similar results were found for the efficiency of detection of the filters. We are thus confident that our method at evaluating the efficiency of detection can be used to compare the filters.

Concerning the Gabor filters, the parameters of Eq. 1 are chosen as follows: the frequency centers  $W$  are 0.061, 0.1, 0.163 and 0.265;  $\sigma_x$  and  $\sigma_y$  are adapted to obtain a filter size with a null DC by multiplying them by a scaling factor.

The only parameter to fix for the Mexican hat filters is  $\sigma$  in Eq. 2. The values used for  $\sigma$  vary from 1 to 5 and are chosen according to a geometric progression. 10 intervals are then created.

The decomposition with the nearly isotropic wavelets  $\phi$  and  $\psi$  contains four levels, as it was the case in the previous studies [1, 2, 3].

### 4.2 Detection of Pointwise Defects

In this section we compare the efficiency of the set of the examined filters for the detection of singularities in Brodatz images and in mammography parts. Let us keep in mind the order of the families of filters according to their sphericity level. The Mexican hat filters are the most spherical. Then the nearly isotropic wavelets are slightly less spherical than the Mexican hat filters. Finally the Gabor filters are the least spherical. For defects with a radius greater than 2 pixels, the order of the filters according to their efficiency at detecting singularities in synthetic images corresponds to the order of their sphericity measure. We here extend this study for the Brodatz textures and the mammography parts.

To increase the significance of the results, the experiment of detection is repeated for five positions of defects, randomly chosen. To satisfy ourselves that the comparison of the results can be generalized, a paired Student test is performed on the results: a first test between the Gabor and the  $\phi$  results, an other between the  $\phi$  and the  $\psi$  results, and a last test between the  $\psi$  and the Mexican hat results. The values of these tests are summarized in table 1(a) for the set of Brodatz images, for which the critical value is 2.32635 since the confidence level is chosen as 0.01 and the degree of freedom is equal to 109 (which effectively corresponds to an infinite degree of freedom). That means that if a value in the table is lower than  $-2.32635$ , the first filter is better than the second one, and if a value in the table is greater than 2.32635, the second filter is better than the first one with great confidence.

Concerning the set of mammography parts, the values of the paired Student tests are summarized in table 1(b). For the same confidence level as the Brodatz images and a degree of freedom equal to 29, the critical value is 2.46202.

**Table 1**  
**Detection of Pointwise Defects: Paired Student Test on**  
**Each Set of Images**

(a) Brodatz textures			
Defect radius	Gabor $\phi$	$\phi$ $\psi$	$\psi$ Mexican hat
1	83.4745	-12.6093	-88.0110
2	62.0286	14.5575	-20.7625
3	38.4730	24.8232	10.9751
4	28.7785	22.4011	7.9366
5	18.4598	22.2813	13.8957
6	14.7884	19.1214	14.9255
7	15.0824	17.0509	12.1155
8	14.2150	19.1356	11.2312
9	11.0677	20.3889	14.5130
10	7.4408	22.6956	18.9155
(b) Parts of mammographies			
Defect radius	Gabor $\phi$	$\phi$ $\psi$	$\psi$ Mexican hat
1	38.2556	16.5524	-35.8688
2	45.7838	13.4464	-3.0051
3	41.9435	15.3969	-1.5875
4	30.4252	20.2203	-6.0870
5	22.0005	18.4412	-3.4675
6	24.3087	11.4936	-4.5371
7	30.5992	8.5238	-7.6913
8	21.5144	8.9753	-9.3811
9	20.1947	12.8953	-8.8334
10	16.3609	14.0923	-5.7940

From table 1(a), we can observe the calculated values of the paired Student tests for the Brodatz images. All the values are significant and a clear tendency is shown for the defects which have a radius greater than 2 pixels: the Mexican hat filters seem to be the most efficient at detecting singularities. The  $\psi$  wavelet is more efficient than the  $\phi$  wavelet, which provides us better results than the Gabor filters. For defects with a radius lower than 2 pixels, the  $\phi$  and  $\psi$  wavelets are more efficient than the Mexican hat filters. All of these observations were also concluded in the case of the synthetic images with a high roughness background [1, 2].

We can explain the poor results of the Gabor filters by the level of sphericity of these filters. Since they are less spherical than the nearly isotropic wavelets, it is unsurprising that their results of detection are worse than those of the  $\phi$  and  $\psi$  wavelets. The same argument can be used to justify the best detection results of the Mexican hat filters, which are the most spherical since they are isotropic.

All this is valid for the defects with a radius larger than 2 pixels. For smaller defects, the form of the  $\phi$  and  $\psi$  wavelets

enables them to adapt to the background better than the Mexican hat filters, and then to detect smaller defects than them.

From table 1(b), we can observe that the Gabor filters are clearly the least efficient to detect singularities in parts of mammographies. The reason is probably the same as for the Brodatz images. In the same way, the nearly isotropic wavelets  $\phi$  and  $\psi$  are still more efficient than the Gabor filters. However, in the case of the mammography parts, the Mexican hat filters are not as much performant as for the Brodatz textures. Their efficiency is then comparable to those of  $\phi$  and the  $\psi$  wavelets. A reason of this tendency is that the form of these wavelets can adapt better to this kind of background than the Mexican hat wavelets. Indeed, the mammography parts seem to be smoother than the Brodatz images. The structure of their texture is more fine.

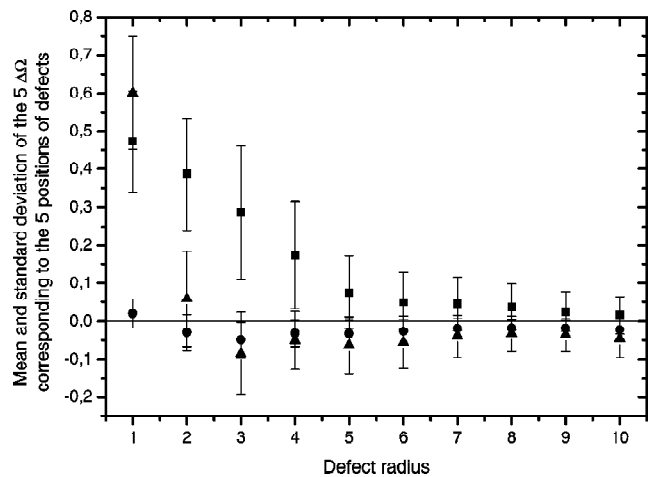


**Figure 8: Detection of pointwise defects in Brodatz textures: comparison of the Gabor filters, the  $\psi$  wavelet and the Mexican hat filters with the  $\phi$  wavelet: (▲) Mexican Hat; (●)  $\psi$ ; (■) Gabor  $\lambda = 1$**

The comparison is then carried out starting from the mean and the standard deviation of the five differences between the results of a filter and those of the reference filter. The reference filter is chosen as the  $\phi$  wavelet. The obtained results are presented in Fig. 8 for the Brodatz images and in Fig. 9 for the parts of mammographies. A negative value means that the filter is more efficient than the filter of reference.

An example of singularity detection is presented in Fig. 10. The first image (a) is the Brodatz image D16 which contains 10 conic defects with a radius of 5 pixels attenuated by a factor  $\Omega$  equal to 0.15. The position of the defects is shown in the second image (b). First the image (a) is processed by the four filters. Four new images are then obtained, and the following steps of the methodology will be performed on them. A threshold is then performed on the processed images in order to extract the interesting points. This threshold can be different for the four filtered images. It is computed to obtain a maximum number of right detected singularities, which are bordered with a square, and a minimum number of wrong detected points (false-positive),

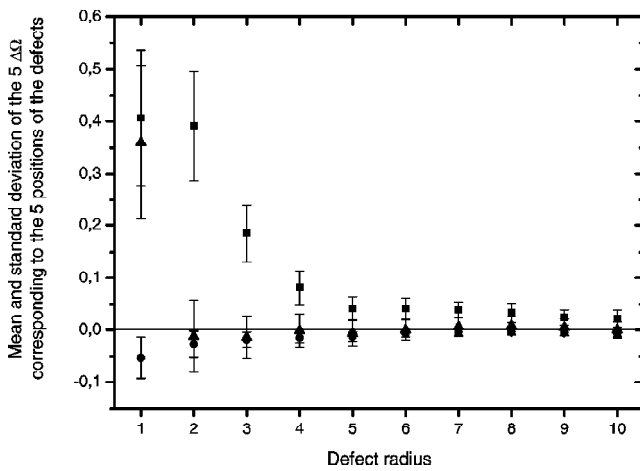


**Figure 9: Detection of pointwise defects in parts of mammographies: comparison of the Gabor filters, the  $\psi$  wavelet and the Mexican hat filters with the  $\phi$  wavelet: (▲) Mexican Hat; (•)  $\psi$ ; (■) Gabor = 1**

bordered with a circle. The image (c) corresponds to the image (a) filtered by the Mexican hat filters after the threshold. The 10 inserted conic defects and no other point are detected. These filters are the most efficient for this case. The images (d) and (e) correspond to the detection with the nearly isotropic wavelets  $\psi$  and  $\phi$ , which are a little less efficient than the preceding filters. Indeed, the 10 defects are still detected, but respectively 1 and 2 false-positives are also observed. Finally, as expected, the Gabor filters give us the lowest number of right detected singularities and the largest number of false-positives, namely 9 right and 9 wrong detected.

### 4.3 Detection of Truncated Singularities

It would be interesting to know if the efficiency of detection of the pointwise singularities is influenced by the top of the cones. In this second part of the experiments, the defects we want to detect are cones without the point at the top. Thus,

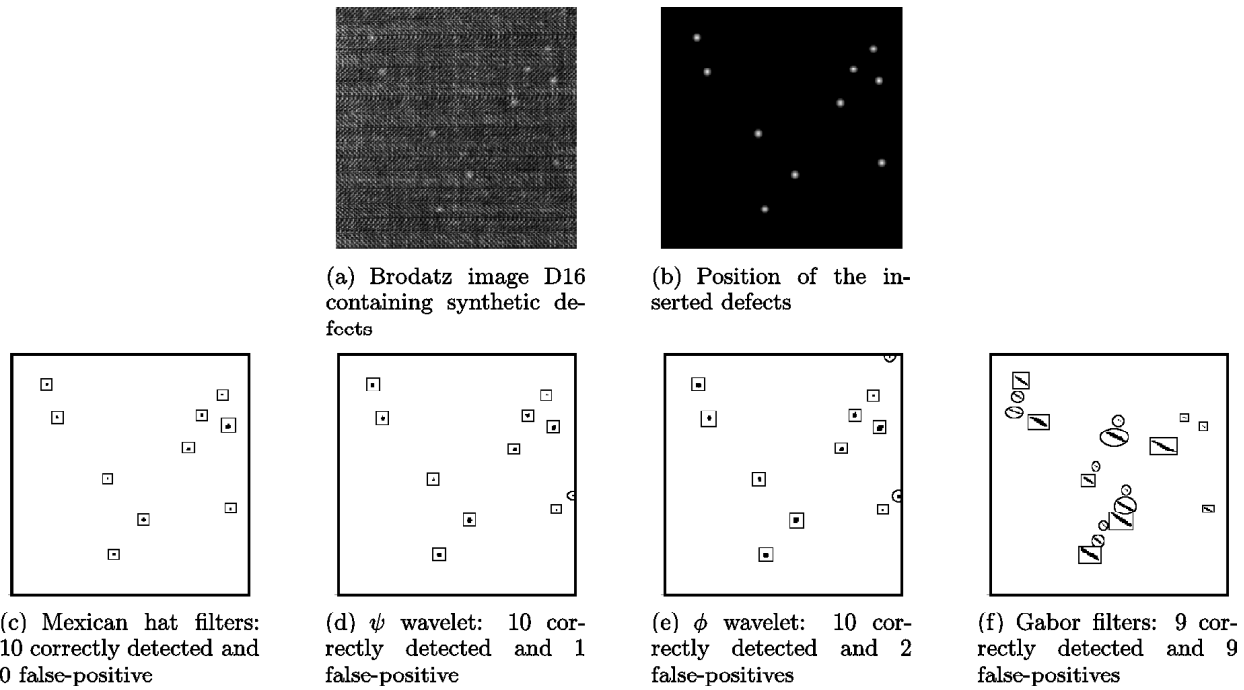


**Figure 10: Example of singularity detection on a Brodatz image**

the defects are truncated at a given height. This new height corresponds to a percentage of the maximal height of the starting cone, i.e. the height between the base and the point of the top. The examined percentages vary from 10 to 100%, a percentage of 100% corresponding to the whole cone. With these tests, the influence of the truncation height on the efficiency of detection is studied.

The other parameter to be examined is the radius of the defects. Two sizes of radius are considered: 20 and 10 pixels. For each size, a paired Student test between the results of the detection for each percentage of truncation, and a summarized graph are presented.

#### 4.3.1 Defects with a radius of 20 pixels

Only one position of defects is sufficient to generalize the results obtained for the detection of truncated defects with a radius of 20 pixels. Indeed, all the values of the paired Student test presented in tables 2(a) and 2(b) are significantly larger than the critical value, which is equal to 2.32635. In table 2(a), corresponding to the Brodatz textures, we can observe that the order of comparison between the filters is not the same as for the pointwise singularities. In this section, the Gabor filters are compared with  $\psi$  the wavelet, which is compared with the  $\phi$  wavelet, which is compared with the Mexican hat filters. The reason of this modification is that

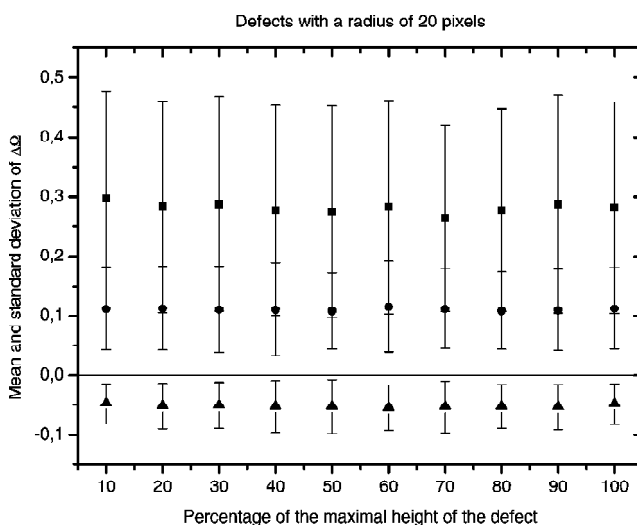
the  $\phi$  wavelet is more efficient than the  $\psi$  wavelet at detecting truncated singularities. We observe the same order of efficiency between the filters whatever is the percentage of truncation. In addition, the Mexican hat filters are always the best at detecting the defects.

**Table 2**  
**Detection of Truncated Singularities with a Radius of 20 Pixels:**  
**Paired Student test on Each Set of Images**

(a) Brodatz textures			
Percentage of height	Gabor $\psi$	$\psi$ $\phi$	$\phi$ Mexican hat
10	13.7549	16.9722	15.1237
20	11.9383	16.8529	14.1157
30	11.8093	16.1139	13.6570
40	11.8561	14.9354	12.6761
50	11.7590	17.7456	12.2797
60	11.3830	15.9574	14.9629
70	12.0089	17.5400	12.8471
80	12.1476	17.5700	14.7675
90	12.0349	16.8586	14.6632
100	11.9913	17.3288	14.8424

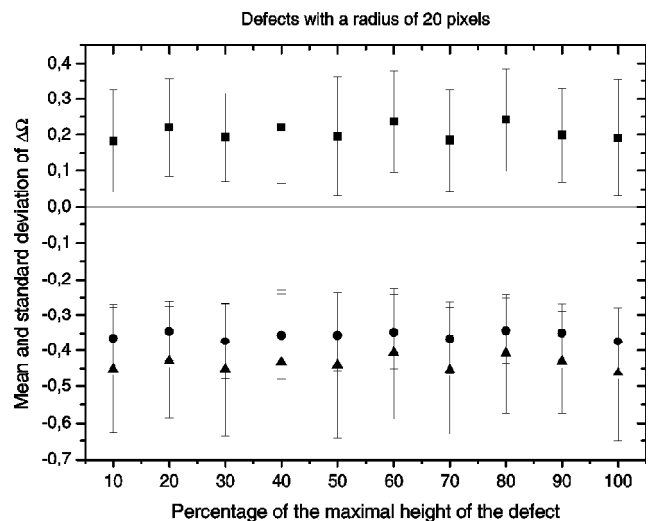
  

(b) Parts of mammographies			
Percentage of height	Gabor $\phi$	$\phi$ $\psi$	$\psi$ Mexican hat
10	7.0089	20.9673	3.8713
20	8.9656	22.5404	3.9322
30	8.6222	19.2651	3.4912
40	7.7957	15.5099	3.6902
50	6.4486	19.1439	3.5331
60	9.1575	18.3983	2.7780
70	7.1718	19.5424	4.2496
80	9.2170	20.3739	3.5230
90	8.3597	23.1228	3.1398
100	6.4319	21.4967	3.9543



**Figure 11: Detection of truncated singularities in Brodatz textures: comparison of the Gabor filters, the  $\psi$  wavelet and the Mexican hat filters with the  $\phi$  wavelet: (▲) Mexican Hat; (●)  $\psi$ ; (■) Gabor  $\lambda = 1$**

All these observations are found again in Fig. 11, which presents a global comparison between the filters and the filter of reference. The values of the graph correspond to the mean and the standard deviation of the difference between the results of a filter and those of the filter of reference. We see that all the values related to the Mexican hat filters are negative, and the others are positive, in the same order. That means that the truncation height of the defects has no effect on the efficiency of detection of the filters, and that the Mexican hat filters are the most efficient, probably because the defects are rather large and the top of those has a spherical aspect, which is also the form of the Mexican hat filters.



**Figure 12: Detection of truncated singularities in parts of mammographies: comparison of the Gabor filters, the wavelet and the  $\psi$  Mexican hat filters with the  $\phi$  wavelet: (▲) Mexican Hat; (●)  $\psi$ ; (■) Gabor  $\lambda = 1$**

In table 2(b), corresponding to the mammography parts, the paired Student tests were performed between the Gabor filters and the  $\phi$  wavelet, the  $\phi$  and  $\psi$  wavelets, and finally between the  $\psi$  wavelet and the Mexican hat filters. The order of detection efficiency between the filters is the same as for the Brodatz images: the Gabor filters are the least efficient, the Mexican hat filters are the most efficient and the nearly isotropic wavelets lie between these two families of filters. Only one difference is observed: in this case, the wavelet is more performant than the  $\phi$  wavelet. The reason of these observations are certainly similar to those for the Brodatz images. The comparison graph is presented in Fig. 12.

#### 4.3.2 Defects with a Radius of 10 Pixels

It would be also interesting to study the influence of the radius of the truncated defects on the detection efficiency of the filters. A second radius is then chosen to be 10 pixels. The same experiment is performed by all the filters, and the analysis of the results is shown in table 3(a) and Fig. 13 for the Brodatz textures and in table 3(b) and Fig. 14 for the parts of mammographies. Let us recall that the critical value is 2.32635 for the set of Brodatz images and 2.46202 for the set of mammography parts.

**Table 3**  
**Detection of Truncated Singularities with a Radius of 10 Pixels:**  
**Paired Student Test on Each Set of Images**

(a) Brodatz textures			
Percentage of height	Gabor $\psi$	$\psi$ $\phi$	$\phi$ Mexican hat
10	4.8459	9.7024	8.6921
20	3.8954	10.6485	8.0611
30	3.3484	9.9598	8.5197
40	3.0231	9.2542	7.6164
50	2.4633	9.8093	8.3562
60	3.9131	9.8578	8.7133
70	3.3169	11.0489	8.2710
80	3.9945	10.3268	7.9023
90	3.9081	11.5180	9.0674
100	3.8329	10.6451	8.3864

(b) Parts of mammographies			
Percentage of height	Gabor $\phi$	$\phi$ $\psi$	$\phi$ Mexican hat
10	7.1417	5.4193	-2.1343
20	9.6817	7.8824	-2.6625
30	7.9257	7.6689	-3.0760
40	7.3414	6.3515	-2.8617
50	8.1466	7.2700	-2.4630
60	9.5615	9.7695	-2.2154
70	5.3057	4.8837	-2.0151
80	9.2192	4.9050	-2.4681
90	10.6547	7.3002	-2.9881
100	8.8315	7.8406	-2.1268

Concerning the Brodatz images, once again we observe the same order of efficiency of detection between the filters: the Mexican hat filters are the most efficient, these are followed by the  $\phi$  and  $\psi$  wavelets, and finally the Gabor filters are the least efficient. The reason of this observation is certainly the same as for defects with a radius of 20 pixels: the large size and the spherical form of the top of the defects seem to be best fitted by the Mexican hat filters. Fig. 13 is used to visualize the comparisons between the examined filters, with the wavelet as reference.

However, concerning the parts of mammographies, the tendency between the nearly isotropic wavelets and the Mexican hat filters is reversed in relation to those observed for the truncated defects with a larger radius. In the present case, the Mexican hat filters seem to be slightly less or as much efficient to detect this kind of defects as the nearly isotropic wavelets. This is probably due to the smaller size of the defects and the regularity of the background, which are more adapted for a detection with the  $\phi$  and  $\psi$  wavelets than the Mexican hat filters.

**5. CONCLUSION**

In this paper, we compare different families of wavelets and filters for the detection of pointwise defects and truncated singularities in Brodatz textures and in parts of mammographies. These families are the Gabor filters, the Mexican hat filters and the nearly isotropic wavelets  $\psi$  and  $\phi$ . The effect of the size of the singularities (as in the preceding work [1, 2]) and the height of the truncation of the truncated defects on the detection are studied. The same procedure of detection is used for the experiments of this work. The aim of this work was to prove that, in terms of detection efficiency, we have the same order between the families of filters on real textured images of reference and on medical images. This assumption is verified by the experiments. Thus we conclude that the Mexican hat filters and the nearly isotropic wavelets are the most efficient for the detection of singularities and other small sized defects for any kind of textured images.

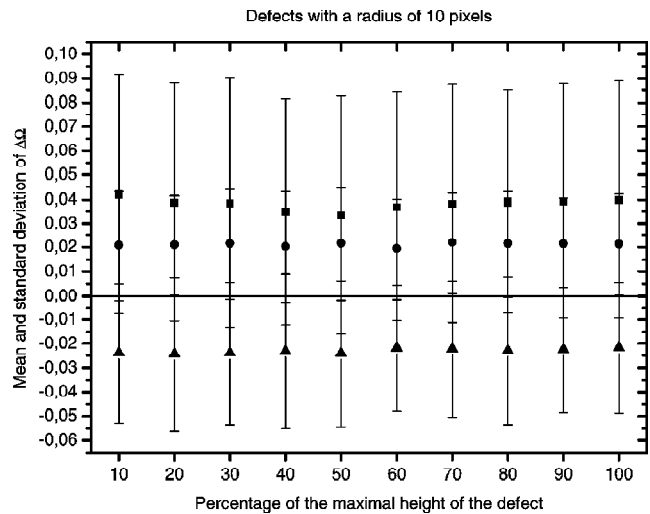


**Figure 13: Detection of truncated singularities in Brodatz textures: comparison of the Gabor filters, the wavelet and the Mexican hat filters with the  $\phi$  wavelet: (▲) Mexican Hat; (●)  $\psi$ ; (■) Gabor  $\lambda = 1$**

**ACKNOWLEDGEMENTS**

This work was completed with the support of the Fonds pour la Formation a la Recherche dans l'Industrie et dans l'Agriculture in Belgium.

**A New separable spherical wavelets**

We will, in this section, describe a method to construct new more spherical wavelets. We will proceed with a numerical optimization. The first step is to isolate the parameters. We will then explain the setup of the optimization procedure we used. We will finally present our results as a Pareto-front. In this paper, we will use both extremes of the used high-pass filter which is isotropic such as explained in [1].

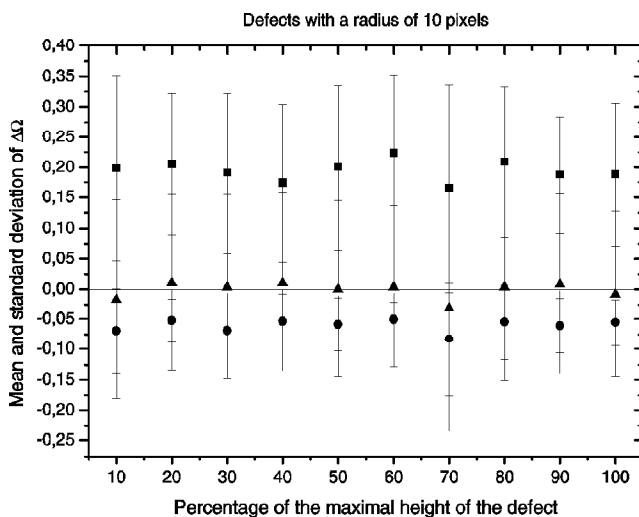


Figure 14: Detection of truncated singularities in parts of mammographies: comparison of the Gabor filters, the  $\psi$  wavelet and the Mexican hat filters with the  $\phi$  wavelet: (▲) Mexican Hat; (●)  $\psi$ ; (■) Gabor  $\lambda = 1$

### A.1 Parametrization

To achieve the parametrization of the set of orthonormal wavelets, we use the algorithm proposed by Sherlock-Monro in [18] which can generate any kind of orthonormal wavelet. For a wavelet with a support width of  $N$ , we have  $N/Z^{-1}$  free parameters. We will use wavelets with a support width of 8 since a quick one-objective optimization of the sphericity of the scaling function with varying support width reveals that essentially no improvement can be obtained with longer wavelets.

### A.2 Optimization

As said above, the compromise between the sphericity of the filters is not known a priori. We are thus looking for a set of solutions representing different trade-offs between the objectives. So, a multiobjective algorithm will be used to optimize the sphericity of both the lowpass and highpass filters. This will allow us to make the compromise between noise removal and high response to defects as described later on. The algorithm we use to perform this multiobjective optimization is a genetic algorithm. This kind of algorithm works with a set of candidate solutions and evolves them to reach the optimum of some fitness function. They can be rather slow, but are robust and can provide good solutions. The evolution is guided through a scalar value attached to each solution, its fitness. The mapping of the two-dimensional objective space to a one-dimensional fitness function needs care. The goal is to reward potentially good individuals but also to maintain diversity. Moreover, we want a well spread set of solutions covering all the Pareto front. The fitness is here computed according to the ‘‘Strength Pareto Evolutionary Algorithm (SPEA)’’ developed by Zitzler and Thiele, see [19]. We did not use elitism to avoid a too fast convergence, even with a population size of 200

but collected the non-dominated individuals of the 100 generations. We then selected 10 wavelets from this optimal set so as to cover the whole Pareto-front. These wavelets will be used throughout this paper.

### A.3 Results

We present in Fig. 15 the Pareto-front, i.e. a set of solutions such that no solution is better in both objectives than another, we obtained from the optimization. Also, two arrows point to two well known wavelets with a support width of 8: the Daubechies and the nearly symmetric wavelets (also called ‘‘least asymmetric’’), see [20] for a complete description of these wavelets, that we here represent by their sphericity.

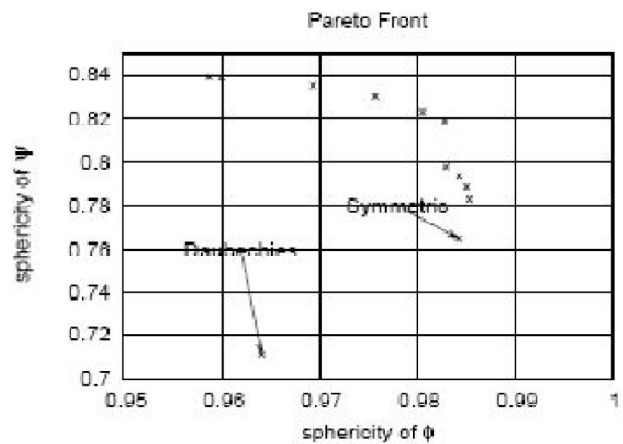


Figure 15: Pareto front generated with GA

### REFERENCES

- [1] C. Gouttiere, G. Lemaure, and J. De Coninck. Influence of filter sphericity on the detection of singularities in synthetic images. *Signal Processing*, 87: 552-561, (2007).
- [2] C. Gouttiere, G. Lemaure, and J. De Coninck. Influence of sphericity parameter on the detection of singularities in synthetic images. In *Computational Modelling of Objects Represented in Images*, pages 211-214, (2007).
- [3] G. Lemaure and J. De Coninck. Sphericity of wavelets may improve the detection of singularities in images. In *Proceedings of Computing Engineering in Systems Applications*, Lille, France, July 2003.
- [4] G. Lemaure. On the Choice of the Wavelet Basis Function for Image Processing. PhD thesis, University of Mons-Hainaut, Belgium, 2003.
- [5] M. Unser. Texture classification and segmentation using wavelet frames. *IEEE Transactions on Image Processing*, 4(11): 1549-1560, (1995).
- [6] Amos Ron, Zuowei Shen, and Kim-Chuan Toh. Computing the sobolev regularity of renable functions by the arnoldi method. *SIAM Journal on Matrix Analysis and Applications*, 23(1): 57-76, 2001.
- [7] G. Lemaure, K. Drouiche, and J. De Coninck. Detection of image singularities using more regular wavelets. In *Wavelet X*, volume 6, San Diego CA, 2003. SPIE.
- [8] G. Lemaure, K. Drouiche, and J. De Coninck. Highly regular wavelets for the detection of clustered microcalcifications in mammograms. *IEEE Transactions on Medical Imaging*, 22: 393-401, (2003).

- [9] H. Ojanen. Orthonormal compactly supported wavelets with optimal sobolev regularity: Numerical results. *Applied and Computational Harmonic Analysis*, 10(1): 93-98, (2001).
- [10] S. Pan, G. Shavit, M. Penas-Centeno, D. H. Xu, L. Shapiro, R. Ladner, E. Riskin, W. Hol, and D. Meldrum. Automated classification of protein crystallization images using support vector machines with scale-invariant texture and Gabor features. *Acta Crystallographica Section D*, 62(3): 271-279, (2006).
- [11] R. Manthalkar, P. K. Biswas, and B. N. Chatterji. Rotation invariant texture classification using even symmetric gabor filters. *Pattern Recognition Letters*, 24(12): 2061-2068, (2003).
- [12] H. Tanaka, Y. Yoshida, K. Fukami, and H. Nakano. Texture segmentation using amplitude and phase information of Gabor filters. *Electronics and Communications in Japan part III-Fundamental Electronic Science*, 87(4): 66-79, (2004).
- [13] D. A. Clausi and H. Deng. Design-based texture feature fusion using Gabor filters and co-occurrence probabilities. *IEEE Transactions on Image Processing*, 14(7): 925-936, (2005).
- [14] D. M. Tsai, C. P. Lin, and K. T. Huang. Defect detection in coloured texture surfaces using Gabor filters. *The Imaging Science Journal*, 53(1): 27-37, (2005).
- [15] K. Muneeswaran, L. Ganesan, S. Arumugam, and K. R. Sundar. Texture classification with combined rotation and scale invariant wavelet features. *Pattern Recognition*, 38(10): 1495-1506, (2005).
- [16] M. Lopez-Caniego, D. Herranz, J. L. Sanz, and R. B. Barreiro. Detection of point sources on two-dimensional images based on peaks. *EURASIP Journal on Applied Signal Processing*, 2005(15): 2426-2436, (2005).
- [17] Y. S. Cheng and T. C. Liang. Rotational invariant pattern-recognition using a composite circular harmonic and 2d isotropic mexican-hat wavelet filter. *Optics Communications*, 112(1-2): 9-15, (1994).
- [18] B. G. Sherlock and D. M. Monro. On the space of orthonormal wavelets. *IEEE Transactions on Signal Processing*, 46: 1716-1720, (1998).
- [19] E. Zitzler and L. Thiele. Multiobjective evolutionary algorithms: A comparative case study and the strength pareto approach. *IEEE Transactions on Evolutionary Computation*, 3(4): 257-271, (1999).
- [20] I. Daubechies. *Ten Lectures on Wavelets*, volume 61 of CBMS-NSF Regional Conference Series in Applied Mathematics. Society for Industrial and Applied Mathematics, Philadelphia, 1992.



This document was created with Win2PDF available at <http://www.win2pdf.com>.  
The unregistered version of Win2PDF is for evaluation or non-commercial use only.  
This page will not be added after purchasing Win2PDF.